

Article

CeO₂ Nanoparticle-Loaded MnO₂ Nanoflowers for Selective Catalytic Reduction of NO_x with NH₃ at Low Temperatures

Shun Li ¹, Zuquan Zheng ², Zhicheng Zhao ³ , Youling Wang ⁴, Yao Yao ³, Yong Liu ^{3,*}, Jianming Zhang ^{1,*}  and Zuotai Zhang ^{2,*}

- ¹ Institute of Quantum and Sustainable Technology (IQST), School of Chemistry and Chemical Engineering, Jiangsu University, Zhenjiang 212013, China; shun@ujs.edu.cn
- ² Guangdong Provincial Key Laboratory of Soil and Groundwater Pollution Control, School of Environmental Science and Engineering, Southern University of Science and Technology, Shenzhen 518055, China; zuquanz@163.com
- ³ Foshan (Southern China) Institute for New Materials, Foshan 528200, China; zhaozhicheng@fscinm.com (Z.Z.); yaoyao@fscinm.com (Y.Y.)
- ⁴ Shunde Graduate School, University of Science and Technology Beijing, Foshan 528399, China; youlingwang@163.com
- * Correspondence: liuy431@gmail.com (Y.L.); zhangjm@ujs.edu.cn (J.Z.); zhangzt@sustech.edu.cn (Z.Z.)

Abstract: CeO₂ nanoparticle-loaded MnO₂ nanoflowers, prepared by a hydrothermal method followed by an adsorption-calcination technique, were utilized for selective catalytic reduction (SCR) of NO_x with NH₃ at low temperatures. The effects of Ce/Mn ratio and thermal calcination temperature on the NH₃-SCR activity of the CeO₂-MnO₂ nanocomposites were studied comprehensively. The as-prepared CeO₂-MnO₂ catalysts show high NO_x reduction efficiency in the temperature range of 150–300 °C, with a complete NO_x conversion at 200 °C for the optimal sample. The excellent NH₃-SCR performance could be ascribed to high surface area, intimate contact, and strong synergistic interaction between CeO₂ nanoparticles and MnO₂ nanoflowers of the well-designed composite catalyst. The in situ diffuse reflectance infrared Fourier transform spectroscopy (DRIFTS) characterizations evidence that the SCR reaction on the surface of the CeO₂-MnO₂ nanocomposites mainly follows the Langmuir–Hinshelwood (L-H) mechanism. Our work provides useful guidance for the development of composite oxide-based low temperature NH₃-SCR catalysts.

Keywords: Mn-Ce mixed oxide; ion-adsorption; selective catalytic reduction; NO_x conversion



Citation: Li, S.; Zheng, Z.; Zhao, Z.; Wang, Y.; Yao, Y.; Liu, Y.; Zhang, J.; Zhang, Z. CeO₂ Nanoparticle-Loaded MnO₂ Nanoflowers for Selective Catalytic Reduction of NO_x with NH₃ at Low Temperatures. *Molecules* **2022**, *27*, 4863. <https://doi.org/10.3390/molecules27154863>

Academic Editors: Caiyun Wang and Long Zhang

Received: 8 June 2022

Accepted: 27 July 2022

Published: 29 July 2022

Publisher's Note: MDPI stays neutral with regard to jurisdictional claims in published maps and institutional affiliations.



Copyright: © 2022 by the authors. Licensee MDPI, Basel, Switzerland. This article is an open access article distributed under the terms and conditions of the Creative Commons Attribution (CC BY) license (<https://creativecommons.org/licenses/by/4.0/>).

1. Introduction

With the fast developing modern industrialization, nitrogen oxides (NO_x) emitted from industrial production and automobile exhaust have become one of the major environmental pollution issues, which may cause acid rain and greenhouse effects [1,2]. Long-term exposure to NO_x can cause several side effects to human health, such as reduced lung function, increased risk of respiratory conditions, and increased response to allergens. As an eco-friendly and efficient approach, selective catalytic reduction of NO_x with NH₃ (NH₃-SCR) is widely used for removing NO_x [3–7]. The core of the NH₃-SCR technology is the catalyst. Although V₂O₅-WO₃(MoO₃)/TiO₂ catalysts have been utilized commercially in the temperature range of 300–400 °C [8], the increasing demands for outstanding catalytic activity at low working temperature with high stability have stimulated the development of novel SCR catalysts.

During the past few decades, enormous research work has been carried out to exploit mixed metal oxides NH₃-SCR catalysts composed of TiO₂, VO_x, MnO_x, CeO₂, Fe₂O₃, ZrO₃ or WO₃ etc., owing to their high stability, strong synergistic interaction, excellent oxygen storage capacity, and redox ability [9–14]. Among all, CeO₂-MnO_x composites with outstanding low-temperature activity, excellent oxygen storage, and release capacity,

and strong mechanical strength, have received considerable attention as a promising candidate $\text{NH}_3\text{-SCR}$ catalyst [15–20]. Nevertheless, $\text{CeO}_2\text{-MnO}_x$ composite catalysts still suffer from several deficiencies in practical applications due to their poor thermal stability, low reduction efficiency, and low sulfur resistance. Considering that the architecture of composite with close contact between each component is crucial for promoting the SCR catalytic activity, considerable work have been conducted to the design and fabrication of hierarchical $\text{CeO}_2\text{-MnO}_x$ composites at nanoscale. For instance, it has been reported that $\text{CeO}_2\text{-MnO}_x$ mixed oxides with hollow structures possess excellent low temperature NO_x storage capacity and $\text{NH}_3\text{-SCR}$ activity owing to the large surface area, rich active sites, and confined micro-environment [21–24]. Therefore, the development of well-designed $\text{CeO}_2\text{-MnO}_x$ composite catalyst with desirable intimate contact at nanoscale is of importance for further enhancing their $\text{NH}_3\text{-SCR}$ catalytic performance.

In this work, a rational designed CeO_2 nanoparticle-loaded MnO_2 nanoflowers (NFs) with adjustable Ce/Mn ratios were prepared through combining a simple hydrothermal and subsequent ion-adsorption-calcination method, as illustrated in Scheme 1. A variety of physical and chemical characterization methods were used to investigate the phase composition, microstructure, and surface characteristics. The unique architecture of the $\text{CeO}_2\text{-MnO}_2$ nanocomposites consisting of MnO_2 nanoflowers loaded with ultrasmall CeO_2 nanoparticles allows the composite with high surface area, intimate contact, and strong synergistic interaction between CeO_2 and MnO_2 . The catalysts displayed excellent low-temperature $\text{NH}_3\text{-SCR}$ activity for NO_x reduction, obtaining a nearly 100% conversion efficiency at 200 °C. Moreover, the $\text{NH}_3\text{-SCR}$ reaction mechanism was revealed by in situ diffuse reflectance infrared Fourier transform spectroscopy (DRIFTs).



Scheme 1. Schematic of the synthesis process for $\text{CeO}_2\text{-MnO}_2$ nanocomposites.

2. Experimental

2.1. Materials

The chemicals of $\text{CeCl}_3 \cdot 7\text{H}_2\text{O}$ (AR, $\geq 99.9\%$), $\text{MnCl}_2 \cdot 4\text{H}_2\text{O}$ (AR, $\geq 99.99\%$), and KMnO_4 (AR, $\geq 99.5\%$) were purchased from Aladdin Reagents and used as received without any further purification. Water was deionized (D.I. water) to reach the Nanopure grade ($18.2 \text{ M}\Omega \cdot \text{cm}$ at 25 °C).

2.2. Synthesis of MnO_2 NFs

MnO_2 NFs were synthesized using a hydrothermal method. Typically, 0.5 g KMnO_4 was dissolved in 50 mL of D.I. water and stirred for 15 min. After that, 1 mol/L $\text{MnCl}_2 \cdot 4\text{H}_2\text{O}$ solution was added into the above solution and stirred for 1 h. Then the mixed solution was transferred into a 100 mL Teflon-lined stainless-steel autoclave and heated in a conventional oven at 100 °C for 12 h. After cooling down to room temperature, the as-obtained powder was washed with D.I. water for three times and dried at 60 °C.

2.3. Synthesis of $\text{CeO}_2\text{-MnO}_2$ Nanocomposites

Typically, 0.1 g of the as-synthesized MnO_2 NFs powder was ultrasonically dispersed in 100 mL of aqueous solution containing certain amount of $\text{CeCl}_3 \cdot 7\text{H}_2\text{O}$ (0.02, 0.04, 0.06, and 0.08 g), denoted as Ce/Mn-1, Ce/Mn-2, Ce/Mn-3, and Ce/Mn-4, respectively. Subsequently, the suspension was magnetically stirred for 24 h to ensure the complete adsorption

of the Ce ions onto the MnO₂ NFs. Then the samples were collected after washing with D.I. water and dried at 60 °C for 12 h. Finally, the as-obtained sample was calcined at different temperatures (300 to 600 °C) for 2 h.

2.4. Materials Characterizations

The crystal structure was investigated by powder X-ray diffraction (XRD) with a Bruker D8 Advance diffractometer (Bruker, Karlsruhe, Germany) with CuK α radiation. The morphology and microstructure were studied by field emission scanning electron microscopy (SEM, Zeiss Merlin, Carl Zeiss NTS GmbH, Oberkochen, Germany) and transmission electron microscopy (TEM, FEI Talos F200X, Thermo Fisher Scientific, Hillsboro, OR, USA), equipped with an energy-dispersive X-ray spectroscope (EDS). X-ray photoelectron spectroscopy (XPS) characterizations were performed using a PHI 5600 XPS system (Perkin-Elmer, Waltham, MA, USA). The obtained spectra were calibrated with the C1s peak at 284.6 eV. The specific surface areas and pore size distributions were estimated by the Brunauer–Emmett–Teller (BET) and Barrett–Joyner–Halenda (BJH) methods with N₂ adsorption and desorption isotherms obtained on a Micrometrics ASAP 2020 system.

2.5. NH₃–SCR Activity Measurement

The SCR activity of the catalysts was evaluated using a conventional fixed-bed quartz microreactor operating in a steady state flow mode under atmospheric pressure. In a typical test, the as-obtained catalysts (50 mg) and quartz sand (200 mg) were mixed and packed between two quartz glass wool plugs. The simulated flue gas composition was NO (500 ppm), NH₃ (500 ppm), O₂ (2%), and balance gas N₂. The total flow rate was 100 mL min^{−1}, which corresponds to a gas hourly space velocity (GHSV) of 16,000 h^{−1}. The concentrations of NO were measured by a chemiluminescence NO_x analyzer (42i-HL, Thermo Scientific). The NO conversion rate was calculated by the following equation:

$$\text{NO}_{\text{conversion}} = \frac{[\text{NO}]_{\text{in}} - [\text{NO}]_{\text{out}}}{[\text{NO}]_{\text{in}}} \times 100\% \quad (1)$$

3. Results and Discussion

3.1. Effect of CeO₂ and MnO₂ Ratio

The CeO₂-MnO₂ nanocomposites with different Ce/Mn ratios were synthesized first. The morphology of the catalysts (taking Ce/Mn-3 as a representative) was characterized by SEM and TEM. As shown in the SEM images (Figure 1a,b), the as-prepared CeO₂-MnO₂ catalyst possesses flower-like morphology with sizes of about 200–300 nm. The TEM images (Figure 1c,d,g) clearly display that the nanoflowers are composed of numerous sheets with thickness of several nanometers. From the HRTEM image (Figure 1e), the interplanar spacings were measured to be 0.32 and 0.70 nm, which can be assigned to the (111) plane of CeO₂ and (001) plane of δ -MnO₂, respectively. The EDS spectrum (Figure 1f) confirms that the composites contain three elements of Ce, Mn, and O, with atomic content of 7.2%, 31.2%, and 61.6%, respectively. Meanwhile, the EDS mapping diagrams (Figure 1h–j) clearly display the homogenous distribution of Mn, Ce, and O elements throughout the NFs, demonstrating the uniform growth of CeO₂ nanoparticles on the MnO₂ NFs. Such a uniform distribution is highly expected to promote their interaction and synergistic effect of Ce and Mn mixed oxides during the catalytic reactions [24,25].

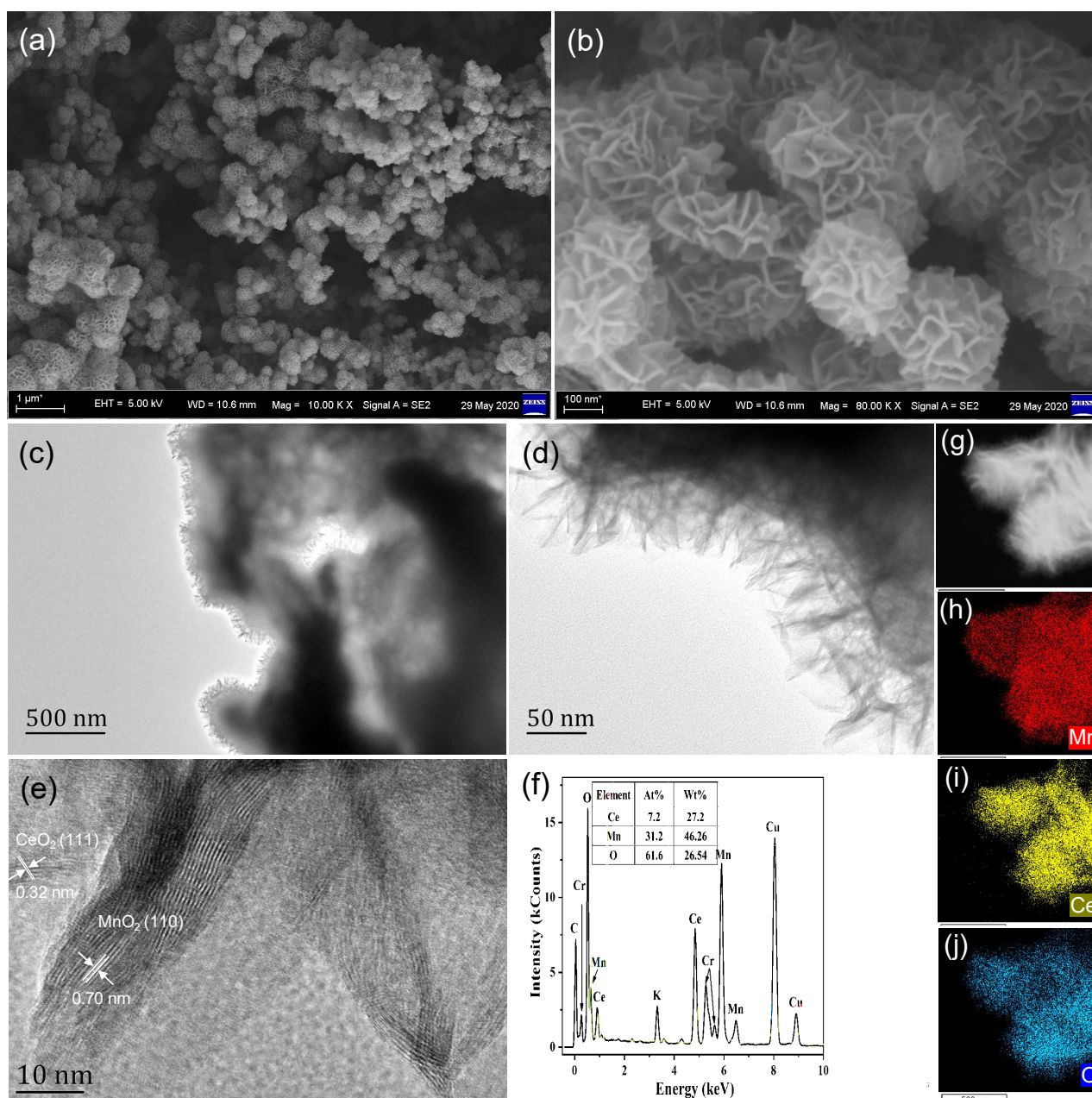


Figure 1. (a,b) SEM, (c) and (d) TEM, (e) HRTEM, (f) EDS spectrum, (g) HAADF-STEM, and (h–j) mapping images of Ce/Mn-3 (300).

The crystal structure of the $\text{CeO}_2\text{-MnO}_2$ catalysts with different Ce and Mn ratios after thermal treatment at $300\text{ }^\circ\text{C}$ was analyzed by XRD. As shown in Figure 2, all diffraction peaks of the pristine MnO_2 sample could be well indexed to $\delta\text{-MnO}_2$ crystal structure (JCPDS No. 80-1098) with predominant crystal planes of (001), (002), and (111). After the adsorption of Ce^{3+} and the following calcination treatment, the diffraction peaks corresponding to CeO_2 (JCPDS No. 81-0792) appeared with predominant crystal planes of (111), (200), and (220), demonstrating the formation of $\text{CeO}_2\text{-MnO}_2$ composites. The peak intensity of CeO_2 gradually increases with the increasing $\text{CeCl}_3\cdot 7\text{H}_2\text{O}$ content. The broad diffraction peaks suggest the small crystal size of the loaded CeO_2 , which is consistent with the TEM observations.

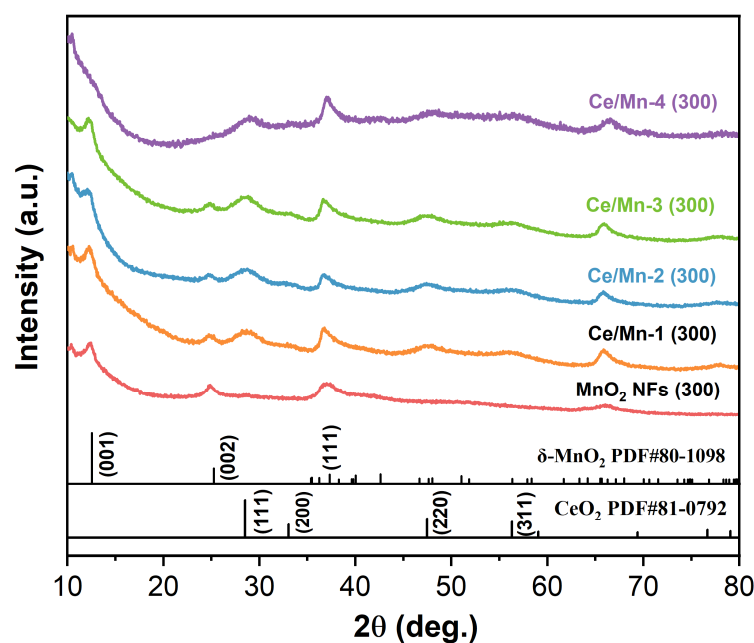


Figure 2. XRD patterns of MnO₂ NFs and CeO₂-MnO₂ composites with different Ce/Mn ratios calcinated at 300 °C.

The NH₃-SCR activity of the as-prepared catalysts calcinated at 300 °C was evaluated. As shown in Figure 3, all the CeO₂-MnO₂ composite catalysts with different Ce and Mn ratios exhibit much higher activity in a relatively wide range of temperature from 50 to 300 °C, compared to pristine MnO₂. As the Ce content increases, the NO conversion rate increases significantly, while decreases at higher Ce contents. Among all samples, Ce/Mn-3 (300) shows the optimal NH₃-SCR catalytic performance, reaching the highest NO conversion rate of about 87.6% at 250 °C.

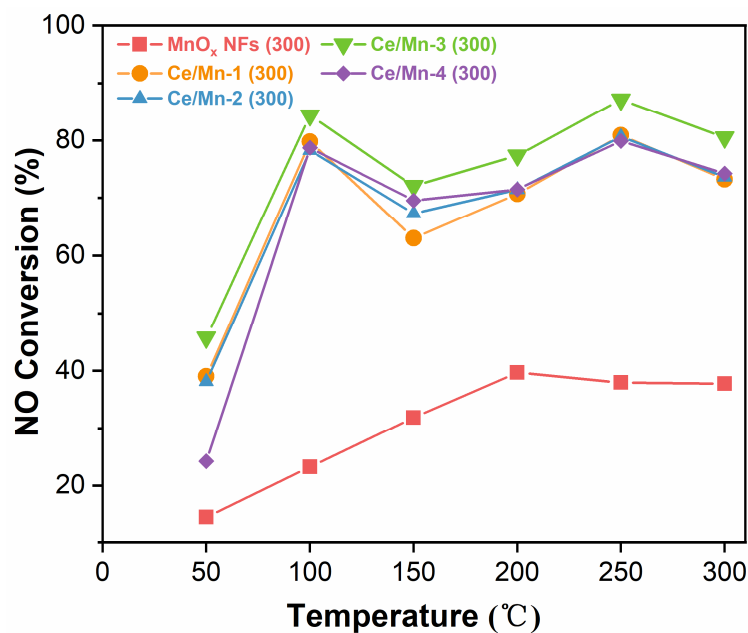


Figure 3. NO conversion curves of MnO₂ NFs and CeO₂-MnO₂ catalysts with different Ce/Mn ratios.

The specific surface areas (SSAs) and pore features are crucial factors determining the catalytic activity. As shown in Figure 4a, the N₂ adsorption–desorption isotherms of the as-prepared catalysts exhibit type IV isotherm with H3 hysteresis loops, demonstrating their mesoporous structure. The CeO₂-MnO₂ composite catalysts possess significantly higher

SSAs in comparison to the pristine MnO_2 , estimated by the BET method. The measured SSAs follow the order of Ce/Mn-3 ($342 \text{ m}^2 \text{ g}^{-1}$) > Ce/Mn-4 ($206 \text{ m}^2 \text{ g}^{-1}$) > Ce/Mn-2 ($154 \text{ m}^2 \text{ g}^{-1}$) > Ce/Mn-1 ($145 \text{ m}^2 \text{ g}^{-1}$) > MnO_2 ($67 \text{ m}^2 \text{ g}^{-1}$). Figure 4b displays the pore size distribution curves estimated by the BJH method. For all samples, the pore size is mostly distributed in the range of 4 to 10 nm, which belongs to the mesoporous structure. The SSAs for the as-prepared CeO_2 loaded MnO_2 NFs are significantly higher than most of the reported CeO_2 - MnO_x nanocomposite catalysts [26–28]. The large SSAs and porous features of the as-synthesized CeO_2 - MnO_2 catalysts (e.g., Ce/Mn-3 (300)) with more catalytic active sites show great advantages for the adsorption and diffusion of gaseous reactants toward high NH_3 -SCR activity [29].

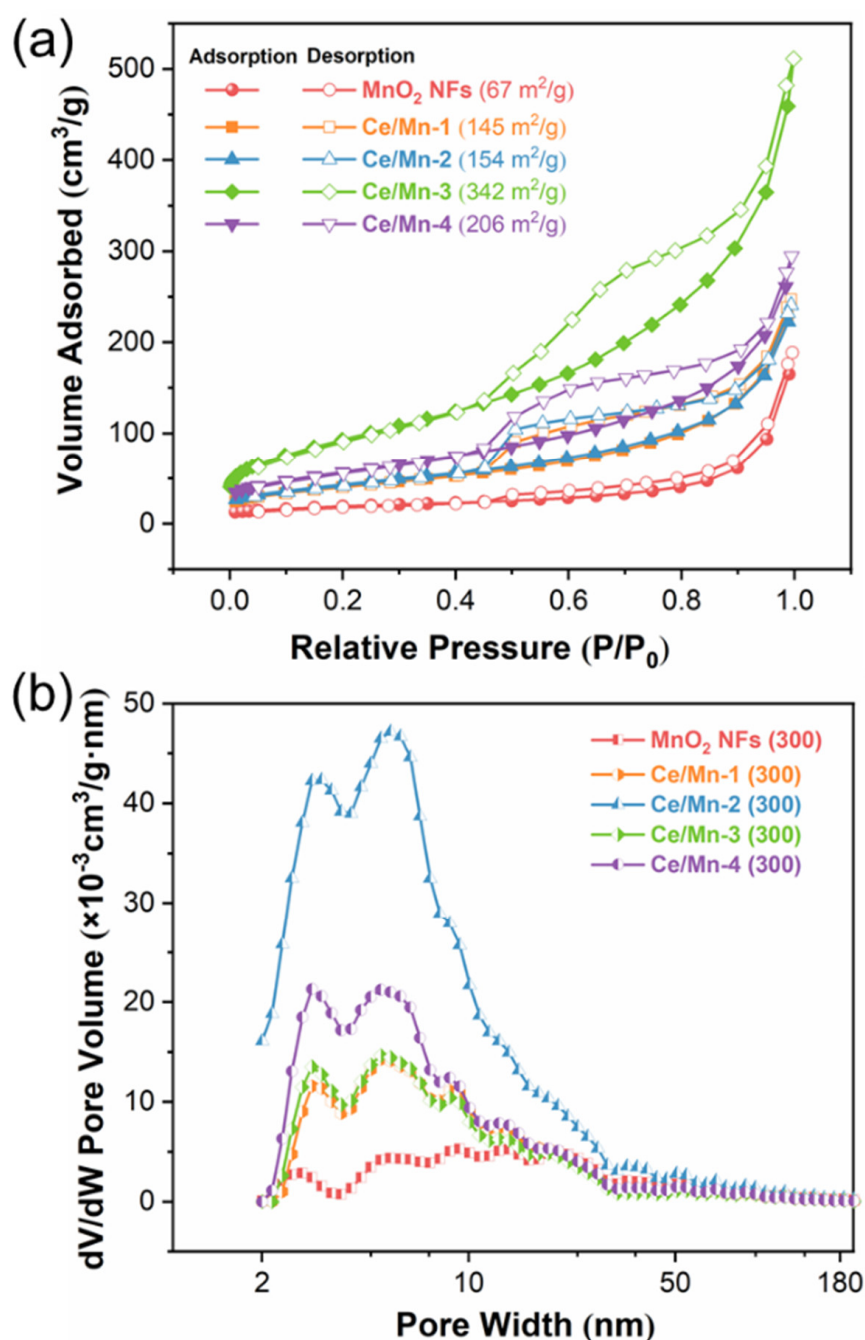


Figure 4. (a) N_2 adsorption–desorption isotherm and (b) pore size distribution of MnO_2 NFs and CeO_2 - MnO_2 catalysts with different Ce/Mn ratios.

3.2. Effect of Thermal Treatment Temperature

To further optimize the NH_3 -SCR catalytic activity of the CeO_2 - MnO_2 composite catalysts, the effect of thermal treatment temperature was investigated, selecting the Ce/Mn-3 sample with the highest activity. Figure 5 displays the XRD patterns of Ce/Mn-3 catalysts after calcinating at four different temperatures of 300 °C, 400 °C, 500 °C, and 600 °C. The samples of Ce/Mn-3 (300), Ce/Mn-3 (400), and Ce/Mn-3 (500) exhibit consistent diffraction peaks, which can be indexed to δ - MnO_2 (JCPDS No. 80-1098) with predominant crystal planes of (001), (002) and (111) and CeO_2 (JCPDS No. 81-0792) with predominant crystal planes of (111), (200), and (220). For the sample treated under 600 °C, secondary phases of Mn_2O_3 (JCPDS No. 89-2809) and Mn_3O_4 (JCPDS No. 75-1560) appeared.

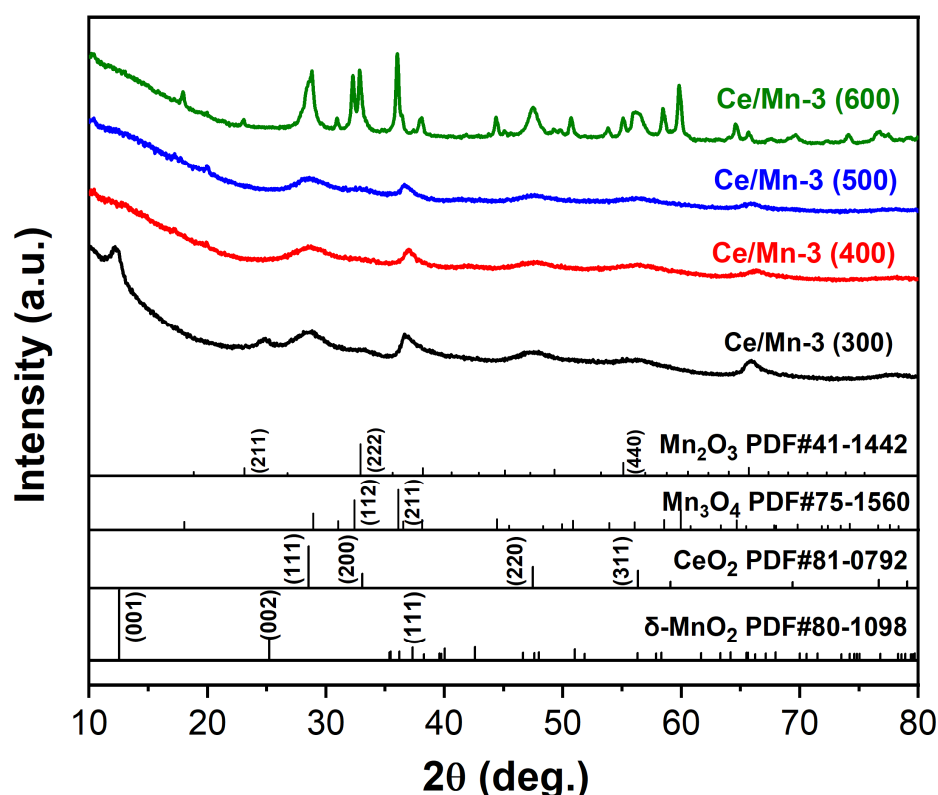


Figure 5. XRD patterns of the Ce/Mn-3 catalysts calcinated at different temperatures.

The SEM images of Ce/Mn-3 catalysts after thermal treatment at different temperatures are displayed in Figure 6. It is clearly shown that spherical flower-like morphology structure was well maintained when the calcination temperature was under 500 °C (Figure 6a–d), compared with that of Ce/Mn-3 (300). Nevertheless, the flower-like hierarchical microstructure of the catalyst for Ce/Mn-3 (600) sample disappeared, forming irregular shaped particles (Figure 6e,f).

Subsequently, the NH_3 -SCR activity of different as-prepared Ce/Mn-3 catalysts were tested. As shown in Figure 7, in the range of 50–200 °C, the NO conversion rate of the catalysts (except for Ce/Mn-3 (300)) increases with the increasement of thermal treatment temperature. Among all the catalysts, Ce/Mn-3 (400) exhibited the highest SCR performance in the low-temperature window from 150 to 300 °C, reaching a 100% removal rate of NO at 200 °C. The activity declined for the catalysts treated at higher temperatures (above 500 °C), which could be ascribed to the changes of structural and surface characteristics of the catalyst, discussed as follows.

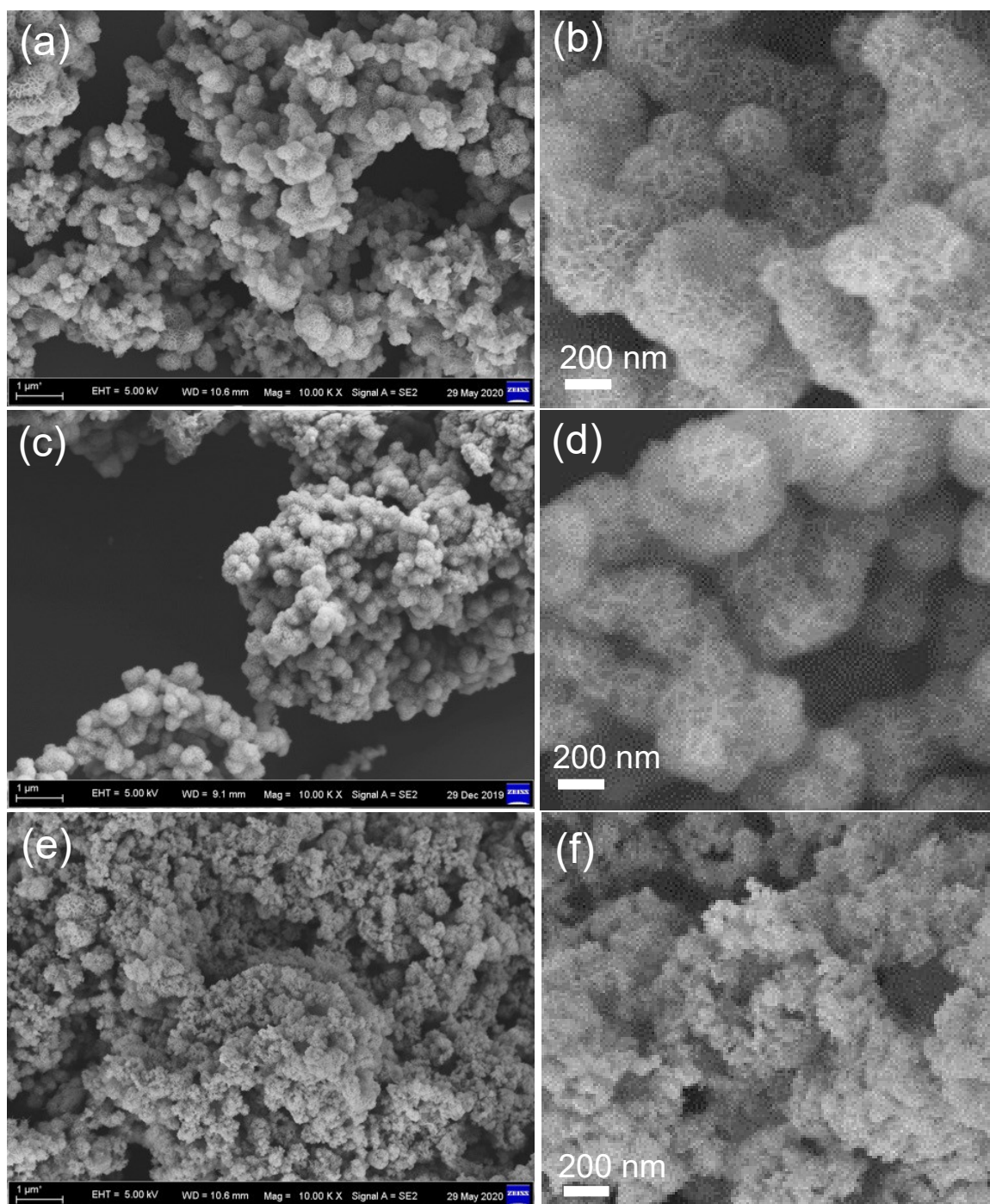


Figure 6. SEM images of the Ce/Mn-3 catalysts calcinated at different temperatures: (a) and (b) 400 °C, (c) and (d) 500 °C, and (e) and (f) 600 °C.

Figure 8 exhibits the N₂ adsorption–desorption isotherms and the pore size distributions of various Ce/Mn-3 catalysts calcinated at different temperatures. From Figure 8a, all the catalysts display IV type N₂ isotherm with H3 type loops, which correspond to the mesoporous structure. Among all samples, the Ce/Mn-3 catalyst prepared at 300 °C has the largest SSA. The SSAs follow the order of Ce/Mn-3 (300) (342 m² g^{−1}) > Ce/Mn-3 (400) (147 m² g^{−1}) > Ce/Mn-3 (500) (97 m² g^{−1}) > Ce/Mn-3 (600) (23 m² g^{−1}). Figure 8b displays the pore size distribution curves estimated by the BJH method, demonstrating that the mesopores are mainly distributed from 4 to 20 nm.

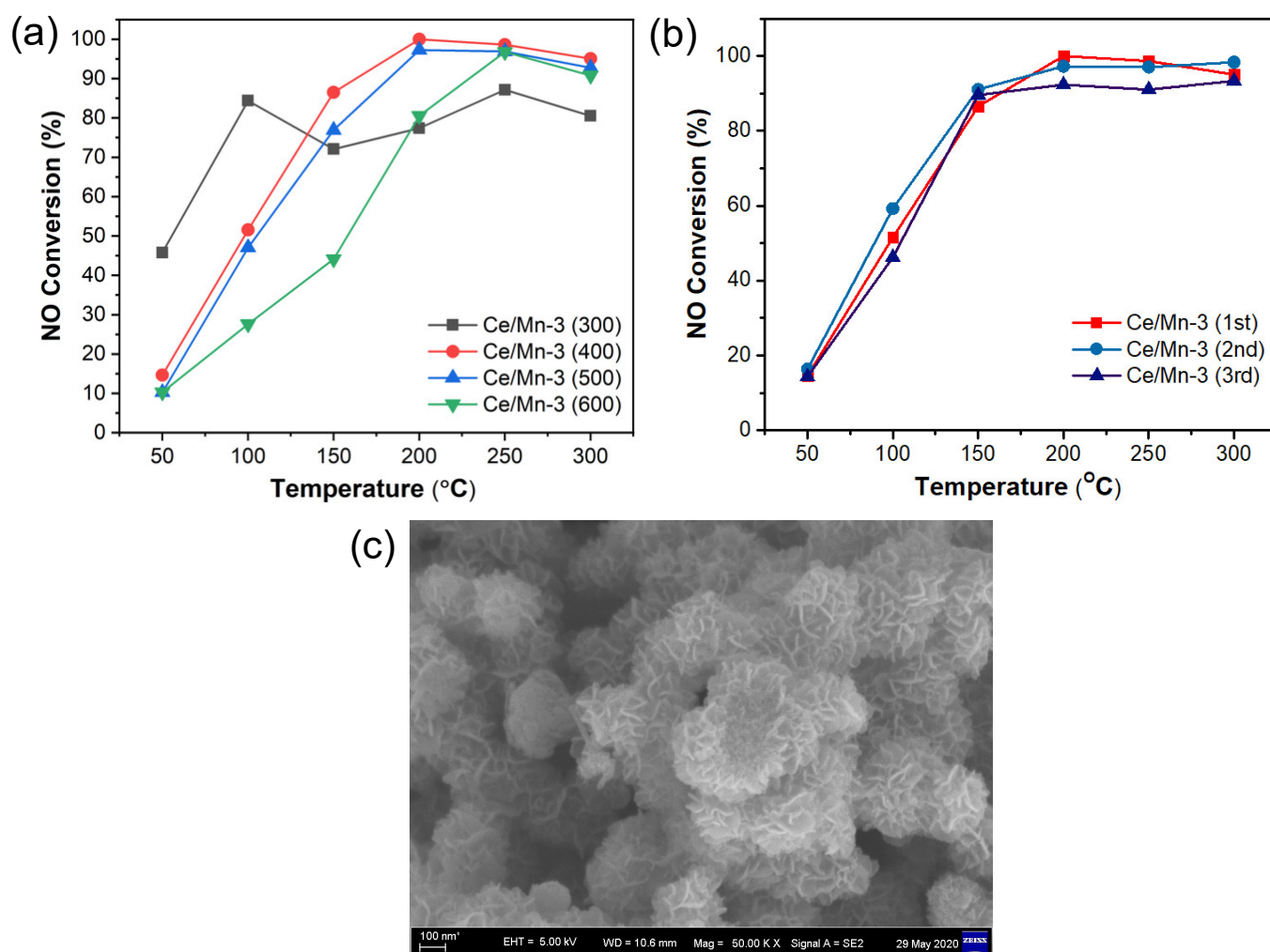


Figure 7. (a) NO conversion curves of the Ce/Mn-3 catalysts calcinated at different temperatures, (b) recycling catalytic activity tests of Ce/Mn-3 (400), and (c) SEM image of Ce/Mn-3 (400) after catalytic reactions.

XPS spectra were measured to analyze the element oxidation states of the composite catalysts calcinated at different temperatures. Figure 9 shows the high-resolution Ce 3d, Mn 2p, and O 1s XPS spectra. As displayed in Figure 9a, the peaks of Ce^{3+} are located at ~ 885.7 eV and ~ 903.1 eV, while the remaining peaks are attributed to Ce^{4+} [30–32]. As listed in Table 1, the calculated Ce^{3+} content (24.84%) in Ce/Mn-3 (400) is the highest among all $\text{CeO}_2\text{-MnO}_2$ samples, which is beneficial for the adsorption of NH_4^+ [33]. In addition, the Mn 2p 3/2 peaks in Figure 9a can be fitted into three peaks, which belong to Mn^{2+} (640.7–641.5 eV), Mn^{3+} (642.2–643.5 eV), and Mn^{4+} (644.8 eV), respectively [34,35]. Generally, Mn with high oxidation states (Mn^{4+}) can promote the oxidation performance of NO over $\text{CeO}_2\text{-MnO}_2$ catalysts at low temperatures. The Ce/Mn-3 (400) catalyst contains more Mn^{4+} (38.55%) than other samples (Table 1), indicating that the catalyst may exhibit outstanding $\text{NH}_3\text{-SCR}$ activity at low-temperature owing to the excellent oxidation ability. Figure 9c shows the XPS spectra of O 1s, which could be deconvoluted into lattice oxygen O_{latt} (~ 529.6 eV), surface oxygen O_{surf} (~ 531.3 eV), and chemically adsorbed oxygen O_{ads} (~ 532.1 eV) [36]. As listed in Table 1, the Ce/Mn-3 sample contains the largest ratio of O_{ads} (23.83%), which has great advantage for the SCR reaction [27,37]. These results are well consistent with the $\text{NH}_3\text{-SCR}$ activity of different catalysts as discussed above.

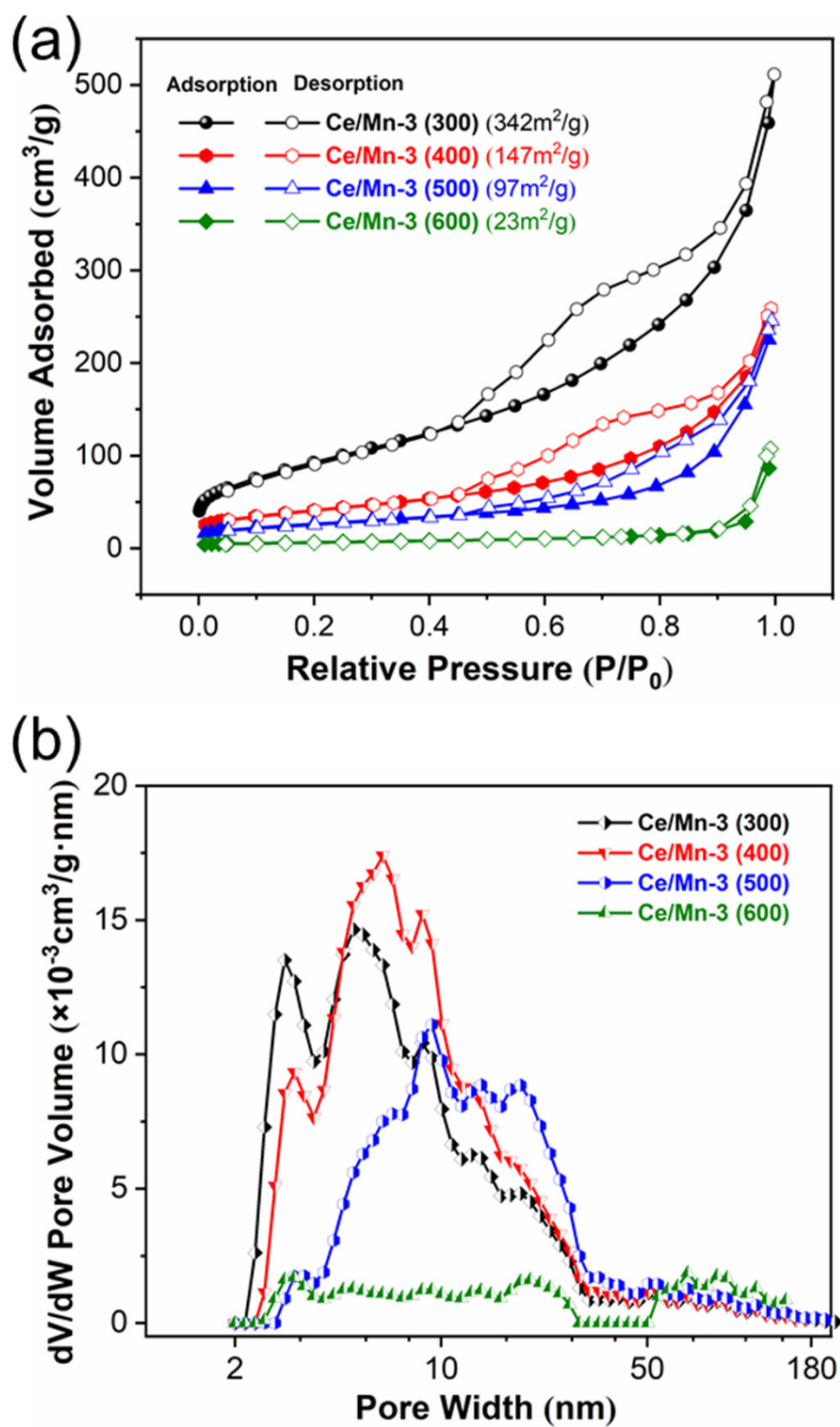


Figure 8. (a) N_2 adsorption–desorption isotherm and (b) pore size distribution of Ce/Mn-3 catalysts calcinated at different temperatures.

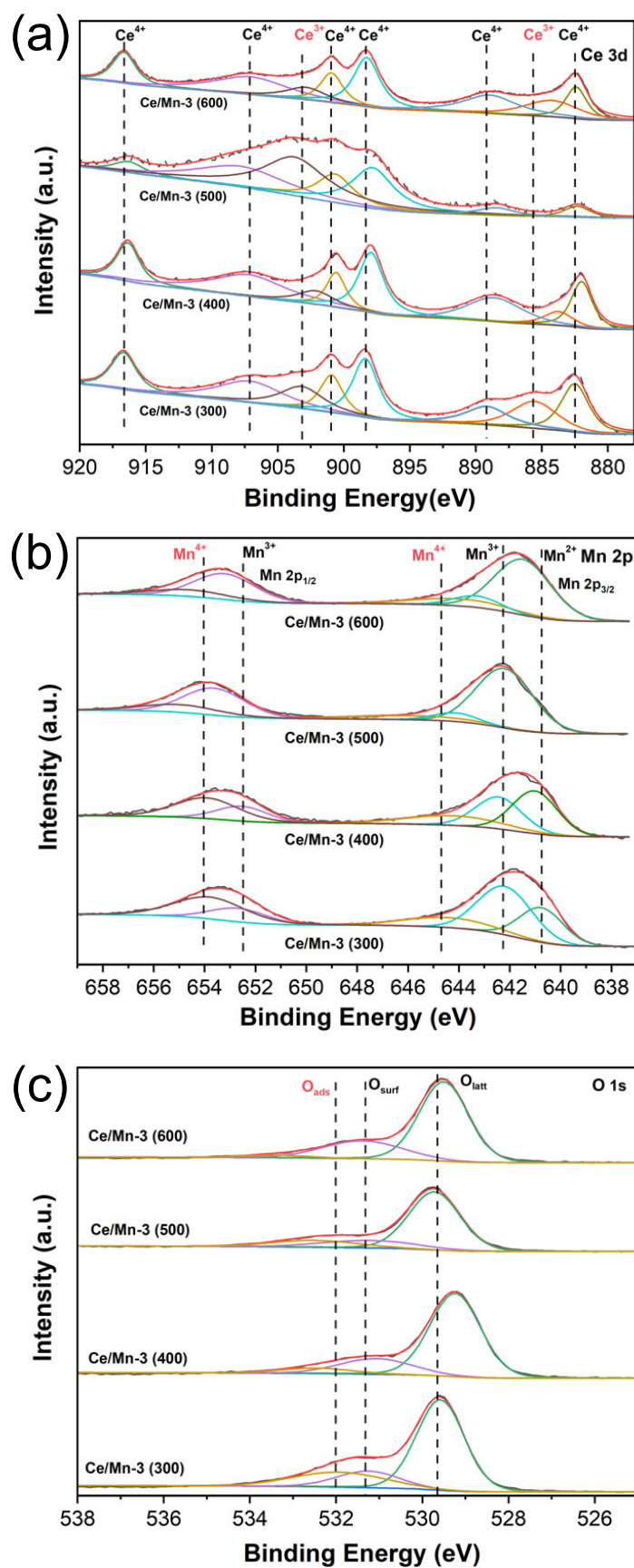


Figure 9. High-resolution XPS spectra of Ce/Mn-3 catalysts calcinated at different temperatures: (a) Ce 3d, (b) Mn 2p, and (c) O 1s.

Table 1. The calculated ratios of Ce^{3+} , Mn^{4+} , and O_{ads} in different catalysts based on XPS analysis.

	Ce^{3+}/Ce (%)	Mn^{4+}/Mn (%)	$\text{O}_{\text{ads}}/\text{O}$ (%)
Ce/Mn-3 (300)	23.79	34.4	19.8
Ce/Mn-3 (400)	24.84	38.55	23.83
Ce/Mn-3 (500)	11.8	17.32	6.47
Ce/Mn-3 (600)	18.94	10.1	2.89

3.3. In Situ DRIFTS Studies

To disclose the NH_3 -SCR reaction mechanism over the CeO_2 - MnO_2 composite catalysts, in situ DRIFTS analysis was conducted by tracking the changes in the adsorbed species on the catalyst (taking Ce/Mn-3 (300) as a representative) surface during the reaction process. Figure 10a shows the NH_3 adsorption DRIFT spectra at 200 °C over the CeO_2 - MnO_2 composite catalyst. The bands at 1692, 1642, and 1458 cm^{-1} belong to the NH_4^+ adsorbed on the Brønsted acid site, while the peaks at 3334, 1626, and 1040–1200 cm^{-1} belong to the NH_3 adsorbed on the Lewis acid site [17,38,39]. In addition, the peaks at 992, 965, and 930 cm^{-1} represent weakly adsorbed gaseous NH_3 on the catalyst's surface. As increasing the adsorption time, the peak at 1458 cm^{-1} belonging to the Brønsted acid site gradually disappeared, indicating that the surface NH_3 adsorption is dominated by the Lewis acid site. The DRIFT spectra of $\text{NO} + \text{O}_2$ adsorption on the CeO_2 - MnO_2 composite catalyst along with the time at 200 °C are presented in Figure 10b. The peaks at 1574, 1530, and 1514 cm^{-1} belonging to nitrates weakened after NO and O_2 were introduced for 30 min, indicating the generation of intermediate products released from the active site to produce N_2 and H_2O [40].

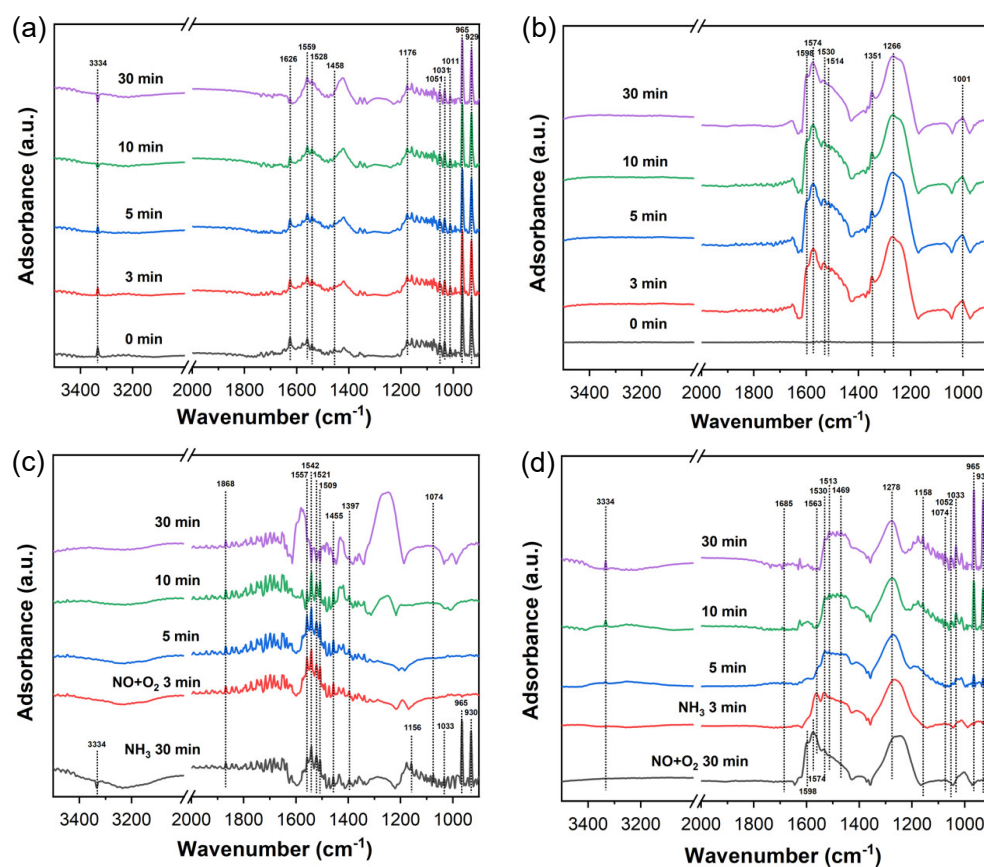


Figure 10. In situ DRIFTS of Ce/Mn-3 (300) at 200 °C over different time: (a) NH_3 adsorption, (b) $\text{NO} + \text{O}_2$ adsorption, (c) reaction of pre-adsorbed NH_3 with $\text{NO} + \text{O}_2$, and (d) reaction of pre-adsorbed NO with NH_3 .

The in situ DRIFT spectra of the CeO₂-MnO₂ catalyst with NO + 5% O₂ reacted with the pre-adsorbed NH₃ at 200 °C are displayed in Figure 10c. Notably, all vibration bands belonging to the adsorbed ammonia species (NH₃ and NH⁴⁺) vanished rapidly after 3 min after introducing NO and O₂, demonstrating the reaction with different ammonia species. The peak at 1455 cm⁻¹ vanished in 30 min, and a new adsorption peak located at 1557 cm⁻¹ assigned to the bipedal nitrate was observed. The peak at 1397 cm⁻¹ could be ascribed to the intermediate species from the surface adsorbed NH₃ and NO_x species. As shown in Figure 10d, the in situ DRIFT spectra were further measured to reveal the reaction of NH₃ with pre-adsorbed NO on the surface of the CeO₂-MnO₂ catalyst at 200 °C. After introducing NH₃, the vibration peaks of weakly adsorbed NO₂ at 1598 and 1574 cm⁻¹ on the surface of Ce/Mn-3 disappeared rapidly. In addition, new vibration peaks at 1685 and 1469 cm⁻¹ owing to the adsorption of NH⁴⁺ at the Brønsted acid site were observed. Additionally, a new adsorption peak at 1513 cm⁻¹ was also detected, which can be ascribed to the bidentate nitrate species resulting from the oxidation of NH₃ by O₂ [9]. Based on the above analysis, we can conclude that the Langmuir–Hinshelwood (L-H) may play an important role in the NH₃-SCR reactions over the CeO₂-MnO₂ composite catalysts because of the formation of a larger amount of adsorbed NH₃ (NH⁴⁺), NO₂, and NH₂ intermediate [9,41].

Moreover, further studies were carried out to reveal the effect of SO₂ and H₂O on the NH₃-SCR catalytic activity of the CeO₂-MnO₂ composite catalyst. The results indicated that the deactivation of the catalyst with the presence of H₂O can be ascribed to the competitive adsorption between NH₃ and H₂O on the Lewis acid sites, which is a reversible process. In the case of SO₂, it will lead to permanent catalyst poisoning through the sulfation of surface active sites. In addition, the competitive adsorption of NO and SO₂ as well as the formation of (NH₄)₂SO₄ on the catalysts' surface may also contribute to the partial deactivation of the CeO₂-MnO₂ catalyst. These conclusions are consistent with previous reports [42]. To regenerate the deactivated CeO₂-MnO₂ catalyst, water washing and thermal or reductive regeneration methods can be used. Further works are still needed to clarify the mechanism of poisoning effect of SO₂ and H₂O and corresponding regeneration methods.

4. Conclusions

In summary, we have synthesized a novel CeO₂-MnO₂ composite catalyst composed of CeO₂ nanoparticles grown on MnO₂ nanoflowers by combining hydrothermal method and ion-adsorption-calcination technique. The unique flower-like hierarchical microstructure and high specific surface area endow the catalysts with desirable intimate contact and synergistic effect, which leads to excellent NH₃-SCR NO_x reduction activity in a wide temperature window from 150 to 300 °C, obtaining a maximal NO conversion of nearly 100% at 200 °C. Moreover, the high contents of Ce³⁺, Mn⁴⁺, and surface O_{ads} in the CeO₂-MnO₂ catalyst could be also responsible for their excellent catalytic performance. Furthermore, in situ DRIFT experiments reveal that the NH₃-SCR reaction route on the surface of the CeO₂-MnO₂ hybrid catalysts is dominated by the L-H mechanism. The as-obtained CeO₂-MnO₂ composites in this work have great prospects for NH₃-SCR reaction of NO_x at low temperatures.

Author Contributions: Conceptualization, S.L.; investigation, Z.Z. (Zuquan Zheng), Z.Z. (Zhicheng Zhao), Y.W. and Y.Y.; resources, Z.Z. (Zuotai Zhang); writing—original draft preparation, S.L.; writing—review and editing, J.Z.; supervision, J.Z. and Y.L.; funding acquisition, S.L. and Y.L. All authors have read and agreed to the published version of the manuscript.

Funding: This work is supported by the Shenzhen Science and Technology Innovation Committee (JCYJ20180504165648211), the National Natural Science Foundation of China (52172187), the Guangdong Basic and Applied Basic Research Foundation (2020A1515110557), the Foshan (Southern China) Institute for New Materials (2021AYF25022), and the startup funding for Jinshan Distinguished professor project of Jiangsu University.

Institutional Review Board Statement: Not applicable.

Informed Consent Statement: Not applicable.

Data Availability Statement: Data is contained within the article.

Conflicts of Interest: The authors declare no conflict of interest.

References

1. Sun, Y.; Zwolińska, E.; Chmielewski, A.G. Abatement technologies for high concentrations of NO_x and SO₂ removal from exhaust gases: A review. *Crit. Rev. Environ. Sci. Technol.* **2016**, *46*, 119–142. [[CrossRef](#)]
2. Gómez-García, M.; Pitchon, V.; Kiennemann, A. Pollution by nitrogen oxides: An approach to NO_x abatement by using sorbing catalytic materials. *Environ. Int.* **2005**, *31*, 445–467. [[CrossRef](#)] [[PubMed](#)]
3. Bosch, F.H. Formation and control of nitrogen oxides. *Catal. Today* **1988**, *2*, 369–379.
4. Kijlstra, W.; Brands, D.S.; Smit, H.I.; Poels, E.K.; Blik, A. Mechanism of the Selective Catalytic Reduction of NO with NH₃ over MnO_x/Al₂O₃. *J. Catal.* **1997**, *171*, 219–230. [[CrossRef](#)]
5. Han, L.; Cai, S.; Gao, M.; Hasegawa, J.-Y.; Wang, P.; Zhang, J.; Shi, L.; Zhang, D. Selective Catalytic Reduction of NO_x with NH₃ by Using Novel Catalysts: State of the Art and Future Prospects. *Chem. Rev.* **2019**, *119*, 10916–10976. [[CrossRef](#)] [[PubMed](#)]
6. Koebel, M.; Madia, G.; Elsener, M. Selective catalytic reduction of NO and NO₂ at low temperatures. *Catal. Today* **2002**, *73*, 239–247. [[CrossRef](#)]
7. Fu, M.; Li, C.; Lu, P.; Qu, L.; Zhang, M.; Zhou, Y.; Yu, M.; Fang, Y. A review on selective catalytic reduction of NO_x by supported catalysts at 100–300 °C—Catalysts, mechanism, kinetics. *Catal. Sci. Technol.* **2014**, *4*, 14–25. [[CrossRef](#)]
8. Lietti, L.; Nova, I.; Forzatti, P. Selective catalytic reduction (SCR) of NO by NH₃ over TiO₂-supported V₂O₅–WO₃ and V₂O₅–MoO₃ catalysts. *Top. Catal.* **2000**, *11*, 111–122. [[CrossRef](#)]
9. Liu, X.; Yu, Q.; Chen, H.; Jiang, P.; Li, J.; Shen, Z. The promoting effect of S-doping on the NH₃-SCR performance of MnO_x/TiO₂ catalyst. *Appl. Surf. Sci.* **2020**, *508*, 144694. [[CrossRef](#)]
10. Zhang, C.; Chen, T.; Liu, H.; Chen, D.; Xu, B.; Qing, C. Low temperature SCR reaction over Nano-Structured Fe-Mn Oxides: Characterization, performance, and kinetic study. *Appl. Surf. Sci.* **2018**, *457*, 1116–1125. [[CrossRef](#)]
11. Forzatti, P. Present status and perspectives in de-NO_x SCR catalysis. *Appl. Catal. A Gen.* **2001**, *222*, 221–236. [[CrossRef](#)]
12. Nova, I.; Lietti, L.; Casagrande, L.; Dall'Acqua, L.; Giamello, E.; Forzatti, P. Characterization and reactivity of TiO₂-supported MoO₃ De-NO_x SCR catalysts. *Appl. Catal. B Environ.* **1998**, *17*, 245–258. [[CrossRef](#)]
13. Busca, G.; Lietti, L.; Ramis, G.; Berti, F. Chemical and mechanistic aspects of the selective catalytic reduction of NO_x by ammonia over oxide catalysts: A review. *Appl. Catal. B Environ.* **1998**, *18*, 1–36. [[CrossRef](#)]
14. Michalow-Mauke, K.A.; Lu, Y.; Kowalski, K.; Graule, T.; Nachttegaal, M.; Kröcher, O.; Ferri, D. Flame-Made WO₃/CeO_x-TiO₂ Catalysts for Selective Catalytic Reduction of NO_x by NH₃. *ACS Catal.* **2015**, *5*, 5657–5672. [[CrossRef](#)]
15. You, X.; Sheng, Z.; Yu, D.; Yang, L.; Xiao, X.; Wang, S. Influence of Mn/Ce ratio on the physicochemical properties and catalytic performance of graphene supported MnO_x-CeO₂ oxides for NH₃-SCR at low temperature. *Appl. Surf. Sci.* **2017**, *423*, 845–854. [[CrossRef](#)]
16. Khan, I.; Sadiq, M.; Khan, I.; Saeed, K. Manganese dioxide nanoparticles/activated carbon composite as efficient UV and visible-light photocatalyst. *Environ. Sci. Pollut. Res.* **2019**, *26*, 5140–5154. [[CrossRef](#)]
17. Qi, G.; Yang, R.T.; Chang, R. MnO_x-CeO₂ mixed oxides prepared by co-precipitation for selective catalytic reduction of NO with NH₃ at low temperatures. *Appl. Catal. B Environ.* **2004**, *51*, 93–106. [[CrossRef](#)]
18. Sun, H.; Park, S.-J. Recent Advances in MnO_x/CeO₂-Based Ternary Composites for Selective Catalytic Reduction of NO_x by NH₃: A Review. *Catalysts* **2021**, *11*, 1519. [[CrossRef](#)]
19. Liu, Z.; Yi, Y.; Zhang, S.; Zhu, T.; Zhu, J.; Wang, J. Selective catalytic reduction of NO_x with NH₃ over Mn-Ce mixed oxide catalyst at low temperatures. *Catal. Today* **2013**, *216*, 76–81. [[CrossRef](#)]
20. Zhang, D.; Zhang, L.; Shi, L.; Fang, C.; Li, H.; Gao, R.; Huang, L.; Zhang, J. In situ supported MnO_x-CeO_x on carbon nanotubes for the low-temperature selective catalytic reduction of NO with NH₃. *Nanoscale* **2013**, *5*, 1127–1136. [[CrossRef](#)]
21. Liu, C.; Gao, G.; Shi, J.-W.; He, C.; Li, G.; Bai, N.; Niu, C. MnO_x-CeO₂ shell-in-shell microspheres for NH₃-SCR de-NO_x at low temperature. *Catal. Commun.* **2016**, *86*, 36–40. [[CrossRef](#)]
22. Zhu, K.; Yan, W.; Liu, S.; Wu, X.; Cui, S.; Shen, X. One-step hydrothermal synthesis of MnO_x-CeO₂/reduced graphene oxide composite aerogels for low temperature selective catalytic reduction of NO_x. *Appl. Surf. Sci.* **2020**, *508*, 145024. [[CrossRef](#)]
23. Ma, K.; Zou, W.; Zhang, L.; Li, L.; Yu, S.; Tang, C.; Gao, F.; Dong, L. Construction of hybrid multi-shell hollow structured CeO₂-MnO_x materials for selective catalytic reduction of NO with NH₃. *RSC Adv.* **2017**, *7*, 5989–5999. [[CrossRef](#)]
24. Feng, J.; Wang, Y.; Gao, D.; Kang, B.; Li, S.; Li, C.; Chen, G. Ce-Mn coordination polymer derived hierarchical/porous structured CeO₂-MnO_x for enhanced catalytic properties. *Nanoscale* **2020**, *12*, 16381–16388. [[CrossRef](#)]
25. Quiroz, J.; Giraudon, J.-M.; Gervasini, A.; Dujardin, C.; Lancelot, C.; Trentesaux, M.; Lamonier, J.-F. Total Oxidation of Formaldehyde over MnO_x-CeO₂ Catalysts: The Effect of Acid Treatment. *ACS Catal.* **2015**, *5*, 2260–2269. [[CrossRef](#)]
26. Jiang, D.; Zhang, M.; Li, G.; Jiang, H. Preparation and evaluation of MnO_x-CeO₂ nanospheres via a green route. *Catal. Commun.* **2012**, *17*, 59–63. [[CrossRef](#)]
27. Wang, X.; Zhao, Z.; Xu, Y.; Li, Q. Promoting effect of Ti addition on three-dimensionally ordered macroporous Mn-Ce catalysts for NH₃-SCR reaction: Enhanced N₂ selectivity and remarkable water resistance. *Appl. Surf. Sci.* **2021**, *569*, 151047. [[CrossRef](#)]

28. Gao, G.; Shi, J.-W.; Liu, C.; Gao, C.; Fan, Z.; Niu, C. Mn/CeO₂ catalysts for SCR of NO_x with NH₃: Comparative study on the effect of supports on low-temperature catalytic activity. *Appl. Surf. Sci.* **2017**, *411*, 338–346. [[CrossRef](#)]
29. Zhao, B.; Ran, R.; Guo, X.; Cao, L.; Xu, T.; Chen, Z.; Wu, X.; Si, Z.; Weng, D. Nb-modified Mn/Ce/Ti catalyst for the selective catalytic reduction of NO with NH₃ at low temperature. *Appl. Catal. A Gen.* **2017**, *545*, 64–71. [[CrossRef](#)]
30. Liu, Z.; Zhu, J.; Li, J.; Ma, L.; Woo, S.I. Novel Mn–Ce–Ti Mixed-Oxide Catalyst for the Selective Catalytic Reduction of NO_x with NH₃. *ACS Appl. Mater. Interfaces* **2014**, *6*, 14500–14508. [[CrossRef](#)]
31. Zhao, S.; Li, S.; Long, Y.; Shen, X.; Zhao, Z.; Wei, Q.; Wang, S.; Zhang, Z.; Zhang, X.; Zhang, Z. Ce-based heterogeneous catalysts by partial thermal decomposition of Ce-MOFs in activation of peroxymonosulfate for the removal of organic pollutants under visible light. *Chemosphere* **2021**, *280*, 130637. [[CrossRef](#)] [[PubMed](#)]
32. Bu, Y.; Chen, Y.; Jiang, G.; Hou, X.; Li, S.; Zhang, Z. Understanding of Au-CeO₂ interface and its role in catalytic oxidation of formaldehyde. *Appl. Catal. B Environ.* **2020**, *260*, 118138. [[CrossRef](#)]
33. Zhang, Z.; Li, R.; Wang, M.; Li, Y.; Tong, Y.; Yang, P.; Zhu, Y. Two steps synthesis of CeTiO_x oxides nanotube catalyst: Enhanced activity, resistance of SO₂ and H₂O for low temperature NH₃-SCR of NO_x. *Appl. Catal. B Environ.* **2021**, *282*, 119542. [[CrossRef](#)]
34. Song, L.; Xu, T.; Gao, D.; Hu, X.; Li, C.; Li, S.; Chen, G. Metal–Organic Framework (MOF)-Derived Carbon-Mediated Interfacial Reaction for the Synthesis of CeO₂–MnO₂ Catalysts. *Chem. Eur. J.* **2019**, *25*, 6621–6627. [[CrossRef](#)]
35. Wang, Z.; Shen, G.; Li, J.; Liu, H.; Wang, Q.; Chen, Y. Catalytic removal of benzene over CeO₂–MnO_x composite oxides prepared by hydrothermal method. *Appl. Catal. B Environ.* **2013**, *138–139*, 253–259. [[CrossRef](#)]
36. Machocki, A.; Ioannides, T.; Stasinska, B.; Gac, W.; Avgouropoulos, G.; Delimaris, D.; Grzegorzczak, W.; Pasieczna, S. Manganese–lanthanum oxides modified with silver for the catalytic combustion of methane. *J. Catal.* **2004**, *227*, 282–296. [[CrossRef](#)]
37. Ali, S.; Chen, L.; Li, Z.; Zhang, T.; Li, R.; Bakhtiar, S.H.; Leng, X.; Yuan, F.; Niu, X.; Zhu, Y. Cu_x-Nb_{1.1-x} (x = 0.45, 0.35, 0.25, 0.15) bimetal oxides catalysts for the low temperature selective catalytic reduction of NO with NH₃. *Appl. Catal. B Environ.* **2018**, *236*, 25–35. [[CrossRef](#)]
38. Huang, X.; Dong, F.; Zhang, G.; Guo, Y.; Tang, Z. A strategy for constructing highly efficient yolk-shell Ce@Mn@TiO_x catalyst with dual active sites for low-temperature selective catalytic reduction of NO with NH₃. *Chem. Eng. J.* **2021**, *419*, 129572. [[CrossRef](#)]
39. Schneider, H.; Tschudin, S.; Schneider, M.; Wokaun, A.; Baiker, A. In Situ Diffuse Reflectance FTIR Study of the Selective Catalytic Reduction of NO by NH₃ over Vanadia-Titania Aerogels. *J. Catal.* **1994**, *147*, 5–14. [[CrossRef](#)]
40. Liu, Z.; Zhang, S.; Li, J.; Ma, L. Promoting effect of MoO₃ on the NO_x reduction by NH₃ over CeO₂/TiO₂ catalyst studied with in situ DRIFTS. *Appl. Catal. B Environ.* **2014**, *144*, 90–95. [[CrossRef](#)]
41. Sun, P.; Huang, S.-X.; Guo, R.-T.; Li, M.-Y.; Liu, S.-M.; Pan, W.-G.; Fu, Z.-G.; Liu, S.-W.; Sun, X.; Liu, J. The enhanced SCR performance and SO₂ resistance of Mn/TiO₂ catalyst by the modification with Nb: A mechanistic study. *Appl. Surf. Sci.* **2018**, *447*, 479–488. [[CrossRef](#)]
42. Pan, S.; Luo, H.; Li, L.; Wei, Z.; Huang, B. H₂O and SO₂ deactivation mechanism of MnO_x/MWCNTs for low-temperature SCR of NO_x with NH₃. *J. Mol. Catal. A Chem.* **2013**, *377*, 154–161. [[CrossRef](#)]